Experimental Realization of a Metamaterial Detector Focal Plane Array

David Shrekenhamer, Wangren Xu, Suresh Venkatesh, David Schurig, Sameer Sonkusale, and Willie J. Padilla

Phys. Rev. Lett. **109**, 177401 — Published 24 October 2012

DOI: 10.1103/PhysRevLett.109.177401

Experimental Realization of a Metamaterial Detector Focal Plane Array

David Shrekenhamer[1]†, Wangren Xu[2]†, Suresh Venkatesh[3],
David Schurig[3], Sameer Sonkusale[2], and Willie J. Padilla[1]⋆
[1]*Department of Physics, Boston College, 140 Commonwealth Ave., Chestnut Hill, MA 02467, USA*
[2]*NanoLab, Electrical and Computer Engineering, Tufts University,*
161 College Ave, Medford, MA, 02155, USA and
[3]*Department of Electrical and Computer Engineering,*
University of Utah, Salt Lake City, UT 84112, USA

We present a metamaterial absorber (MMA) detector array that enables room-temperature, narrow-band detection of gigahertz (GHz) radiation in the S-band (2-4 GHz). The system is implemented in a commercial printed circuit board process and we characterize the detector sensitivity and angular dependence. A modified MMA geometry allows for each unit cell to act as an isolated detector pixel and to collectively form a focal plane array (FPA). Each pixel can have a dedicated microwave receiver chain and functions together as a hybrid device tuned to maximize the efficiency of detected power. The demonstrated sub-wavelength pixel shows detected sensitivity of -77 dBm, corresponding to a radiation power density of 27 nW/m^2, with pixel to pixel coupling interference below -14 dB at 2.5 GHz.

PACS numbers:

Engineered artificial materials consisting of sub-wavelength, periodic metallic inclusions, can exhibit exotic electromagnetic properties not readily available in nature. Over the past decade, interest of the scientific and engineering communities for developing such metamaterial structures has been continuous and increasing. Experimental realizations of negative index of refraction [1, 2], invisibility cloaks [3], and perfect lensing [4] all served to ignite the field. As metamaterial research continues to mature, demonstrations of practical devices will become increasingly important for continued growth. Metamaterial based sources, detectors and modulators that could be used in communication systems, or for imaging and sensing applications, would go far to validate the initial promise of the technology. Thus far several modulator designs have been experimentally demonstrated [5–7], but the development of metamaterial based sources and detectors is lacking [8, 9].

Microwave imaging systems working between 8-30 GHz have been used for decades in remote sensing and radio astronomy [10, 11]. Common designs are often notably massive and bulky, employing mechanical positioning stages (to raster scan a single pixel across an image plane to build up an image), or using an array of efficient but very substantial elements, such as horn antennas [12]. Though the greatest gains in performance come from increasing the aperture, if compactness, mobility or inconspicuousness are desirable, one would like to have an imaging system that maximizes the performance and minimizes the weight and bulk at a given aperture size. With pixel spacing on the order of the diffraction limited spot size $a \sim \lambda_0/2\pi$ (where λ_0 is the wavelength of the radiation at the imaging frequency), the focal plane can be adequately sampled and all available information acquired. However, such dense spacing is at odds with pixel channel independence. Minimizing cross-talk between detector pixels can require spacings that result in poor resolution and sparse spatial sampling of the image [13–15]. Achieving a high detected-to-incident power efficiency is another key aspect to consider in order to improve the sensitivity. Ideally, one would like to transfer all power to the detector that is incident within the boundaries of a pixel. In all examples to-date there are trade-offs between power efficiency and pixel independence [16, 17]. We believe that resonators developed in the metamaterial community can offer different and potentially superior options for pixel density, channel independence and power efficiency.

In this letter, we present a metamaterial absorber (MMA) that operates as a detector of microwave radiation. Each MMA unit cell functions as an individual antenna coupled detector and, collectively, as a focal plane array (FPA). The metamaterial unit cell converts the incident microwave radiation into electric currents, which are guided to a dedicated receiver chain and finally detected with a power detector to produce DC voltage linearly proportional to the signal. All metamaterial elements and receiver system components can be integrated into a single printed circuit board (PCB).

The ability of metamaterial unit cells to completely absorb incident electromagnetic energy – with effectively zero reflected signal – has been demonstrated across much of the electromagnetic spectrum [18–20], and have shown great potential for use in applications ranging from thermal emitters [21] to energy harvesting [22]. One key design feature afforded by metamaterials is the ability to engineer materials for matching the impedance of the MMA to that of free space. The resonant nature of the MMA structures generates high electric fields in the gap, completely dissipating the incident energy into a combination of dielectric and ohmic losses [23, 24]. However, here we modify the MMA design in order to instead

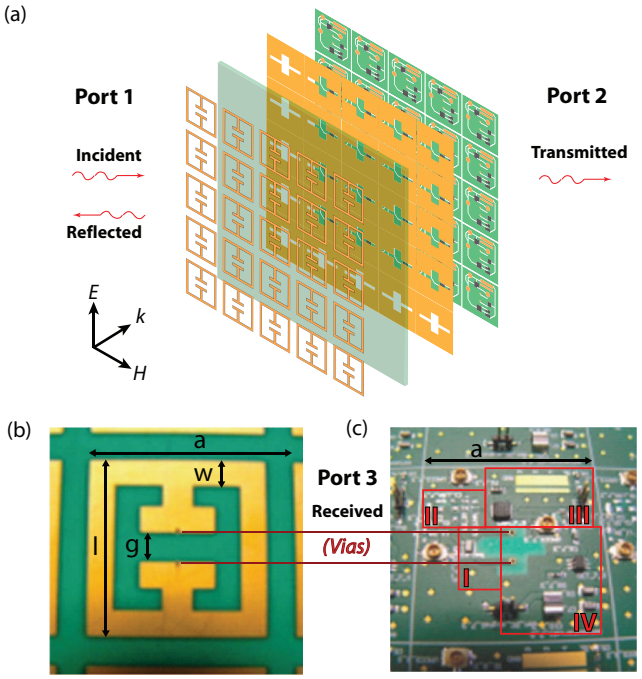

FIG. 1: (Color online) System architecture of our metamaterial microwave power detector array. (a) Radiation is incident from port 1 with electric field polarization as depicted. A schematic of the full device is shown (exploded view) and the layers shown from top to bottom are: the ELC, Rogers dielectric spacer, patterned ground plane, and microwave power receiver circuit. (b) Photo of an individual pixel, i.e. an ELC unit cell with dimensions of $a = 27.3$, $l = 24$, $w = 3.5$, and $g = 4$; all in millimeters. (c) Photo of the circuit layer with *vias* indicated. The *vias* transport the received signal (port 3) to the microwave power receiver circuit underneath each unit cell where the different highlighted regions are: (I) balun, (II) impedance matching circuit, (III) low noise amplifier, and IV) microwave power detector.

transfer the incident energy into a detector circuit. We have utilized the highly absorbing capability of the MMA to fashion a focal plane array by letting each individual unit cell serve as an array elements.

The microwave FPA presented here consists of metamaterial unit cells arranged on a square lattice of 11 by 11 elements. The entire detector system architecture – all contained within the footprint of each unit cell – consists of the metamaterial absorber followed by a balun, impedance matching circuit, low noise amplifier (LNA) and a microwave power detector. The FPA has been implemented in a twelve layer commercial PCB process fabricated and assembled by Hughes circuits, including four metal layers and *vias*, see Fig. 1. The device is constructed from a 30.5 μm copper layer which constitutes the electrically coupled LC (ELC) resonators [25, 26], followed by a patterned ground plane, power routing plane, and the circuit layer – where the ELC and ground plane are separated by Rogers 4003 dielectric with a 4.88 mm thickness. Microwave radiation received by the metamaterial perfect absorber is transferred by the 0.5 mm diameter *vias* to the circuit layer where a balun is used to transform the balanced signal to an unbalanced signal. The signal is then fed into the impedance matching circuit which not only maximizes the signal power, but also serves to compensate for variances in the MPA resonance frequency – due to imperfections in the fabrication process. Finally the signal is amplified by the LNA before being converted to a DC signal by the microwave power detector.

We simulate the entire detector array using commercial 3D electromagnetic simulation software CST's Microwave Studio 2011. The ports, (shown schematically in Fig. 1), are used to investigate the transfer of electromagnetic energy in the device and consist of waveguide ports (port 1 and 2), and a discrete port (port 3). The discrete port is a lumped circuit element that connects the *vias* to one another with a defined impedance set equal to 100 Ohms (Ω), which is equivalent to the input impedance of the balun. The metamaterial was configured to maximize the transfer of energy into port 3, i.e. S_{31}, while at the same time minimize both the free space reflection coefficient (S_{11}) and reflection coefficient (S_{33}) at 2.0 GHz. In order to achieve this goal we tuned the dimensions of the MMA; consisting of the ELC geometry, thickness of the Rogers 4003 ($\tilde{\varepsilon} = \varepsilon_1 + i\varepsilon_2 = 3.38 + i0.007$) dielectric spacer, and the opening in the ground plane. The final dimensions of the ELC resonator are shown in Fig. 1(b) with parameters as labeled. The dimensions of the cross shaped opening in the ground plane, (Fig. 1(c)), were optimized to minimize the coupling between the *vias* and ground plane, as well as tune the MMA's effective magnetic response. The ground plane also helps to shield any undesirable coupling effects between the circuit components and the metamaterial's electromagnetic performance.

The simulated scattering parameters are shown in Fig. 2(a) and demonstrate that a maximum in transmission corresponds with the minima of both reflection coefficients S_{11} and S_{33} at 2.0 GHz. As mentioned, the MMA design typically utilizes the dielectric and ohmic losses within the constituent components in order to achieve a minimum in S_{11}. In contrast, the design presented here achieves S_{31}= 0.986, indicating that over 97% of the incident intensity is transmitted into the detector circuit. In Fig. 2(b) we plot the surface current density at resonance and find that our MMA achieves a response similar to prior designs [25]. Fig. 2(c) shows the magnitude of the electric field and, as can be observed, the electric field is focused into the ELC split gap (right panel) and the *vias* are sufficiently decoupled from the ground plane.

Although simulations presented above indicate that a high performance MMA unit cell may be used as a detector of incident radiation, tolerances in both the component values and the geometry can occur in the fabrication

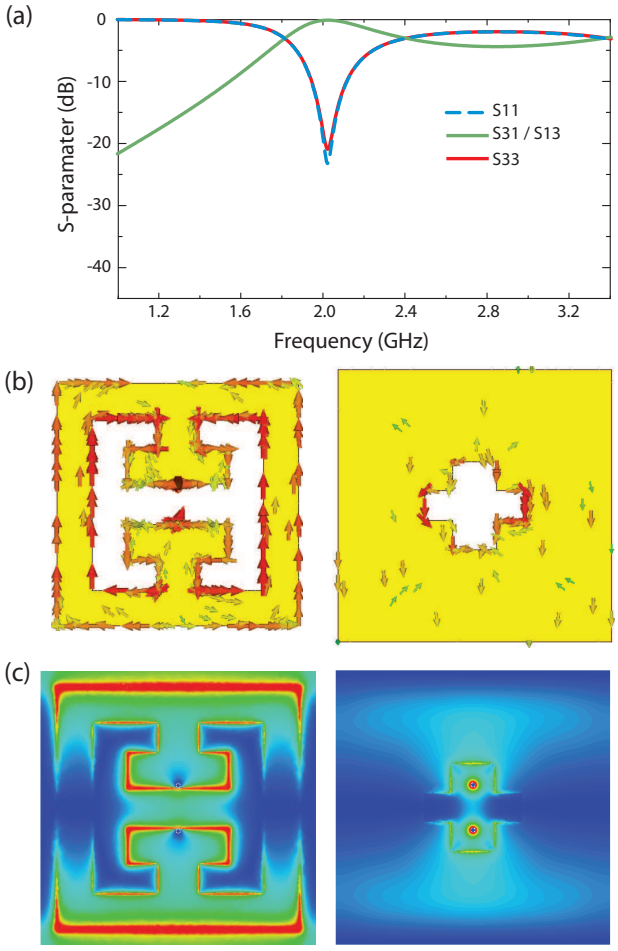

FIG. 2: (Color online) Numerical simulations of metamaterial absorber. (a) Simulated results of the free space reflection (S_{11} dashed blue curve), transmission (S_{31} green curve), and reflection coefficient (S_{33} red curve). Simulated current densities (b) and electric field magnitude (c) shown directly underneath the ELC (left) and above the ground plane (right) at the simulated design frequency of 2.0 GHz.

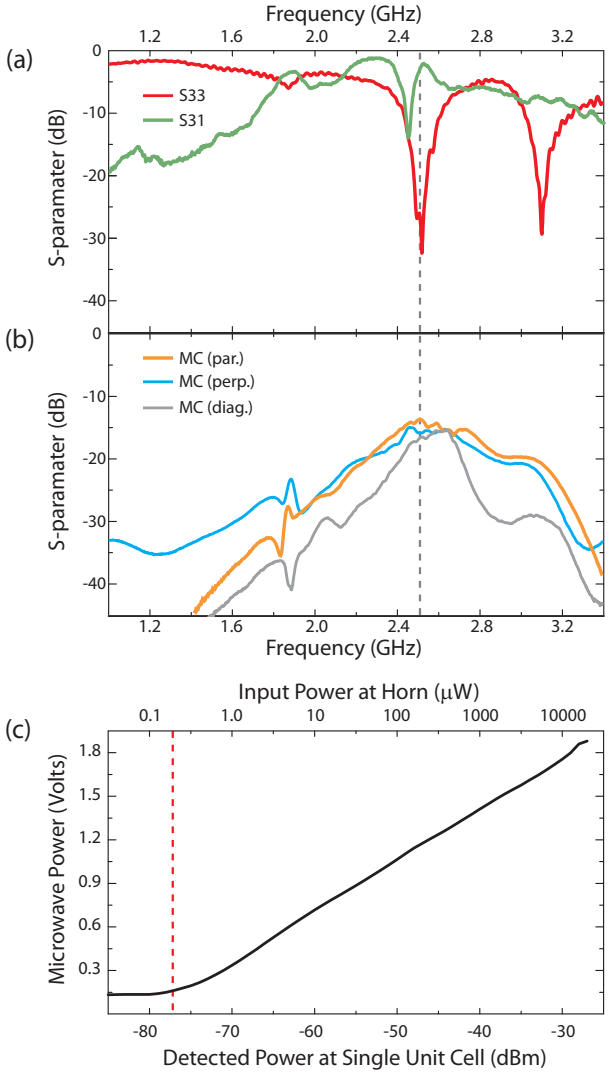

FIG. 3: (Color online) Experimental measurements in anechoic chamber for the center pixel on the MMA / FPA. (a) S-parameter data shows the reflection coefficient (S_{33} red curve) and the transmission (S_{31} green curve) with the dashed grey line at 2.5 GHz the frequency for sensitivity and off-angle measurements. (b) Mutual coupling (MC) between neighboring metamaterial pixels located parallel (gold curve), perpendicular (blue curve), and diagonal (grey curve) with respect to the electric field polarization. (c) Sensitivity characterization with the output of microwave power detector of single pixel as function of incident power, and is sensitive as indicated by dashed red line down to -77 dBm at 2.5 GHz.

process and may thus alter the ideal electromagnetic response. Characterization of S_{11} is not possible with our experimental setup. However, simulations presented in Fig. 2(a) indicate that S_{33} is a reasonable approximation of S_{11}. Thus we measure S_{33} in order to investigate the resonant properties of the fabricated MMA, shown as the red curve in Fig. 3(a). We observe a high reflection coefficient across the range investigated but notably minima occur at 2.5 and 3.15 GHz, with values of -33 dB and -29 dB, respectively. The simulated minimum in S_{33} occurring at 2.0 GHz has shifted to 2.5 GHz, which we attribute to the variation in the fabrication from the simulated design (see the Supplemental Material [27] for more details).

Free space measurements of the center pixel were performed within an anechoic chamber (see the Supplemental Material [27] for more details). We use a HP 8510B vector network analyzer (VNA) with a double ridge guide horn antenna (700 MHz - 18 GHz range) as a transmitter. The horn was connected to a port of the VNA which provided a power level of -3 dBm. Another port of the VNA was directly connected following the unbalanced signal output of the balun on the center single pixel of the MMA / FPA. The resulting S-parameters measured

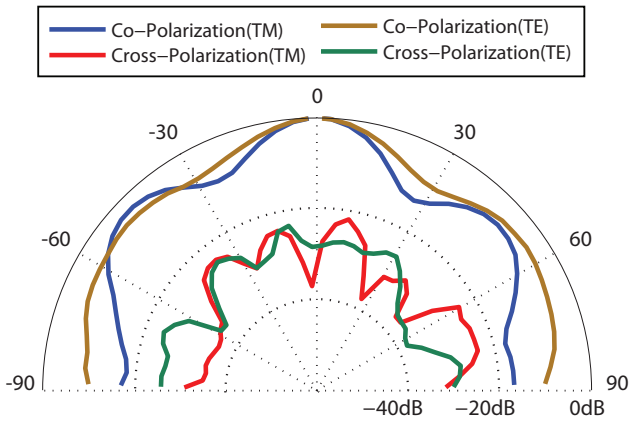

FIG. 4: (Color online) (Color online) Off-angle performance characterization of the MMA / FPA at 2.5 GHz for both the electric field vector perpendicular (TE) and parallel (TM) to the floor of the chamber. The ELC resonator's are rotated between the correct polarization (E-field perpendicular the split gap) and the cross polarization (E-field parallel to the gap).

were for only this center pixel with all neighboring unit cells having 50 Ω terminations following their respective balun output connections. The MMA / FPA was placed 1.75 m away from the horn antenna to be in the far field of the horn's radiating field pattern. In Fig. 3(a), the green S_{31} curve shows a peak about 2.5 GHz overlapping with the minimum observed in S_{33}.

The gold curve in Fig. 3(b) displays the measured mutual coupling (MC) between neighboring unit cells parallel to the electric field direction. At 2.5 GHz the MC was measured to be below -14 dB. We have also measured the MC in the perpendicular and diagonal neighboring cells and mutual coupling of -15 dB was found. Values of MC are significantly low, especially considering the proximity of nearest neighbors at a lattice spacing of $\lambda/4.4$ (27.3 mm) and with edge separation of $\lambda/40$ (3.0 mm). In addition to the clear benefit toward imaging, [13–15] reducing MC is of particular importance for multiple input multiple output (MIMO) communication systems that suffer reduction in channel capacity due to these affects [28, 29].

We now turn toward characterization of the sensitivity and angular dependence of the MMA / FPA. A microwave source was fixed to operate at 2.5 GHz and fed to the horn antenna. The DC voltage output from the MMA / FPA was recorded as the horn power was swept from -50 dBm to +20 dBm as shown in Fig. 3(c). We determine an ultimate pixel sensitivity of -77 dBm, corresponding to a radiation power density of 27 nW/m^2, after calibrating for cable and free space losses. Fig. 4 shows the resulting off-angle performance characterization of the MMA / FPA at 2.5 GHz for both transverse electric (TE) and transverse magnetic (TM) polarizations. However it should be noted that our metamaterial does not posses 90° rotational symmetry and thus we characterized TE and TM for both the "correct" polarization – as shown in Fig. 1(a) – the cross polarization to this. The measurement results demonstrate that the MMA / FPA operates as a wide angle antenna. This is consistent with the off-angle absorption performance typical to MMAs [24]. Both TE and TM cross-polarized angular dependent measurements are at minimum of 20dB lower that the co-polarized measurements. Thus the presented MMA / FPA may be used for polarization discrimination imaging.

The metamaterial absorber focal plane array was demonstrated to operate at 2.5 GHz and have high pixel sensitivity of -77 dBm, with low pixel to pixel coupling interference below -14 dB, good frequency selectivity and wide angular performance. We note that the FPA is not restricted to the frequency applied in this work but could prove useful at higher frequency operation from microwave to millimeter wave. Even more generally, the MMA due to its ability to capture nearly all of the incident electromagnetic energy at design frequencies across the entire electromagnetic spectrum could serve as an excellent candidate to act as detector pixels when implemented into bolometric or semiconducting configurations. The sub-wavelength unit cell and narrow resonant spectral bandwidth can also be expanded to enable multicolor and co- and cross-polarized pixels.

† David Shrekenhamer and Wangren Xu contributed equally to this work. We acknowledge support from the Office of Naval Research under U.S. Navy Contract No. N00014-07-1-0819, the Department of Energy under grant number DE-SC0005240, and the National Science Foundation under grant number ECCS-1002340.

[1] R. A. Shelby, D. R. Smith, and S. Schultz, Science 292, 77 (2001).

[2] D. R. Smith, W. J. Padilla, D. C. Vier, S. C. Nemat-Nasser, and S. Schultz, Phys. Rev. Lett. 84, 4184 (2000).

[3] D. Schurig, J. J. Mock, B. J. Justice, S. A. Cummer, J. B. Pendry, A. F. Starr, and D. R. Smith, Science 314, 977 (2006).

[4] J. B. Pendry, Phys. Rev. Lett. 85, 3966 (2000).

[5] H. -T. Chen, S. Palit, T. Tyler, C. M. Bingham, J. M.O. Zide, J. F. O'Hara, D. R. Smith, A. C. Gossard, R. D. Averitt, W. J. Padilla, N. M. Jokerst, and A. J. Taylor, Appl. Phys. Lett. 93, 091117 (2008).

[6] H. -T. Chen, W. J. Padilla, J. M. O. Zide, A. C. Gossard, A. J. Taylor, and R. D. Averitt, Nat. Photonics 3, 148 (2009).

[7] D. Shrekenhamer, S. Rout, A. C. Strikwerda, C. Bingham, R. D. Averitt, S. Sonkusale, and W. J. Padilla, Opt. Express 19, 9968 (2011).

[8] H. Tao, E. A. Kadlec, A. C. Strikwerda, K. Fan, W. J. Padilla, R. D, Averitt, E. A. Shaner, and X. Zhang, Opt. Express 19, 21620 (2011).

[9] F. B. P. Niesler, J. K. Gansel, S. Fischbach, and M. Wegener, Appl. Phys. Lett. 100, 203508 (2012).

[10] http://www.skatelescope.org.

[11] C. Carilli and S. Rawlings, *Science with the square kilometre array* (North-Holland, Amsterdam, 2004), 48.

[12] R. Appleby and R. N. Anderton, Proc IEEE 95, 1683 (2007).

[13] J. P. Weem and Z. Popovic, IEEE MTT S Int. Microwave Symp. Dig. 3, 271 (2001).

[14] C. Craeye, B. Parvais, and X. Dardenne, IEEE transactions on antennas and propagation 52, 3245 (2004).

[15] K. F. Warnick and M. A. Jensen, IEEE transactions on antennas and propagation 53, 2490 (2005).

[16] M. V. Ivashina, M. Kehn, P. -S. Kildal, and R. Maaskant, Proc. EuCAP, 1 (2006).

[17] M. N.M. Kehn, M. V. Ivashina, P. -S. Kildal, and R. Maaskant, AEU-Int. J. Electron. Commun. 64, 403 (2009).

[18] N. I. Landy, S. Sajuyigbe, J. J. Mock, D. R. Smith, and W. J. Padilla, Phys. Rev. Lett. 100, 207402 (2008).

[19] H. Tao, N. I. Landy, S. M. Bingham, X. Zhang, R. D. Averitt, and W. J. Padilla, Opt. Express 16, 7181 (2008).

[20] J. M. Hao, J. Wang, X. L. Liu, W. J. Padilla, L. Zhou, and M. Qiu, , Appl. Phys. Lett. 96, 251104 (2010).

[21] X. Liu, T. Tyler, T. Starr, A. F. Starr, N. M. Jokerst, and W. J. Padilla, Phys. Rev. Lett. 107, 045901 (2011).

[22] K. Aydin, V. E. Ferry, R. M. Briggs, and H. A. Atwater, Nat. Commun. 2, 517 (2011).

[23] X. Liu, T. Starr, A. F. Starr, and W. J. Padilla, Phys. Rev. Lett. 104, 207403 (2010).

[24] H. Tao, C. M. Bingham, A. C. Strikwerda, D. Pilon, D. Shrekenhamer, N. I. Landy, K. Fan, X. Zhang, W. J. Padilla, and R. D. Averitt Phys. Rev. B 78, 241103 (2008).

[25] D. Schurig, J. J. Mock, and D. R. Smith, Appl. Phys. Lett. 88, 041109 (2006).

[26] W. J. Padilla, M. T. Aronsson, C. Highstrete, M. Lee, A. J. Taylor, and R. D. Averitt, Phys. Rev. B 75, 041102 (2007).

[27] See Supplemental Material for a detailed description of the materials and methods of fabrication, experiment, and numerical simulations.

[28] M. A. Jensen and J. W. Wallace, IEEE Trans. Antennas Propagat. 52, 2810 (2004).

[29] C. -Y. Chiu , C. -H. Cheng , R. D. Murch, and C. R. Rowell, IEEE Trans. Antennas Propag. 55, 1732 (2007).